Int. J. Heat Mass Transfer. Vol. 31, No. 2, pp. 397–405, 1988
Printed in Great Britain

0017–9310/88 $3.00 + 0.00

Optical CT measurement and mathematical prediction of multi-temperature in pulverized coal combustion field

K. OHTAKE and K. OKAZAKI
Department of Energy Engineering, Toyohashi University of Technology, Tempaku-cho, Toyohashi 440, Japan

(*Received* 1 *September* 1987)

Abstract—Temperature distributions of particles and gas in the pulverized coal combustion furnace were measured by a newly developed CT (computer tomographic) technique in which the particle temperature was measured by an instantaneous two color pyrometry and the gas temperature by a wing zone Na-D line reversal method. A simplified mathematical model was formulated for a one-dimensional pulverized coal combustion field with the radiative heat transfer processes of scattering, absorbing and emitting. The model calculations predicted that the particle temperature was more than 400 K higher than the gas temperature, especially in the region of volatile matter combustion. This result explained the phenomena actually observed by the optical measurements well.

1. INTRODUCTION

THE COMBUSTION mechanisms of pulverized coal are affected by the complex interwoven relations between heat and mass transfer and chemical reactions. Radiative heat transfer has the greatest effect on the temperature histories of coal particles and this causes the temperature difference between particles and gas. Evaluation of the actual temperature realized in the pulverized coal combustion fields is urgently desired, not only to study the detailed combustion mechanisms of this complicated media, but also to design the high performance boiler furnaces with low emission of pollutants.

Recently, significant temperature differences between particles and gas in the pulverized coal combustion process have been experimentally shown [1] to be up to 400 K. This was measured in an electrical furnace into which pulverized coal particles were introduced in limited number density so that the individual particles did not interfere with each other. The wall temperature there might be lower than the actual pulverized coal combustion temperature and the temperature differences between particles and gas in the real combustion media could be expected to be higher than the reported value.

The radiative heat transfer process in the scattering and absorbing media has been analyzed by Love and Grosh [2] and Hisia and Love [3] by solving simplified radiative heat transfer equations. The scattering effect has been studied by Steward and Guruz [4] and Wall *et al.* [5] using the Monte Carlo simulation for a cylindrical furnace. However, the temperature history of burning coal particles has not been analyzed nor discussed. Kansa and Perlee [6], Mussara *et al.* [7] and Jost *et al.* [8] have analyzed the time-dependent changes of flame structure around the burning coal particles, but no scattering effect is considered in their analyses.

In this study, the authors intend to evaluate the particle and gas temperatures and their differences and to clarify the scattering effect on the temperature history in the actual pulverized coal combustion process. A newly developed optical CT (computer tomographic) technique was applied to measure the particle and gas temperature distributions in a pulverized coal combustion field and a simplified mathematical model formulated for the pulverized coal combustion field with radiative heat transfer processes, including scattering, absorbing and emitting, was analyzed.

2. PARTICLE AND GAS TEMPERATURE MEASUREMENTS BY OPTICAL CT METHOD

The measurement of particle and gas temperatures in pulverized coal combustion fields is required to understand the detailed combustion mechanisms of coal particles not only with regard to fundamental research, but also in connection with practical pulverized coal combustion devices. A few ideas [9, 10] to measure these temperatures in the practical devices have been tried, however, there always exist some difficulties or restrictions. Some could not separate the particle temperature from the gas one, and some could not decide the temperature distributions.

This study adopted the newly developed optical CT technique to determine the temperature distributions in pulverized coal combustion fields.

2.1. *Principle of measurement*

In order to reconstruct the local particle and gas temperature distributions in pulverized coal com-

NOMENCLATURE

B	local radiative intensity [W m^{-2}]	SR	oxygen–fuel stoichiometric ratio
d_p	particle diameter [m]	T_g	gas temperature [K]
E	emissive power [W m^{-2}]	T_L	brightness temperature of source light [K]
I	transmitted light intensity [W m^{-2}]	T_p	particle temperature [K]
I_0	incident light intensity [W m^{-2}]	t	time [s]
K	attenuation coefficient [m^{-1}]	VM	volatile matter content [wt.%, dry base]
L	optical path length [m]	X	particle size parameter.
m	complex refractive index		
N	particle number density [m^{-3}]	Greek symbols	
n	refractive index	κ	absorption index
Q_a	absorption efficiency factor	λ	wavelength [m]
Q_e	extinction efficiency factor	Φ	phase function of scattering [sr^{-1}]
Q_s	scattering efficiency factor	ω_s	albedo of scatter.

bustion fields by an optical CT method, every optical intensity obtained must be corrected by considering the attenuation caused by the loaded particles and the absorbing gases. In this method the following three independent diagnostics were simultaneously applied to the same measuring section. The first was for the measurement of attenuation coefficient distributions across the cross-sectional area which could be obtained by the attenuation of introduced He–Ne laser light intensity. The second was the instantaneous two colored pyrometry at 650 and 900 nm to determine the particle temperature distributions across the same measuring plane. The light intensities obtained were fed back to the local emitting intensities while considering the attenuation coefficient distributions obtained above. The local particle temperature distributions were evaluated by the usual calculation method of two color pyrometry from thus obtained local emitting intensities. The third was for the gas temperature distributions by an Na-D line reversal method in which three kinds of information had to be measured. These were the transmitted light source intensity of the Na-D line through the measuring zone, the light intensity of the Na-D line from the same zone and the Na-D line intensity from the light source. These measured light intensities were also attenuated by the absorption of sodium gas and the loaded particles. We must therefore calculate these intensities back to the local ones by considering again the attenuation effects. These procedures are shown in Fig. 1 as a flow diagram.

2.1.1. *Distributions of extinction coefficient.* The distributions of the attenuation coefficient along the optical path were determined by projection profiles of the four He–Ne laser beams introduced in the measuring plane. The applicability of Beer's law was certified by the cold flow experiment. The transmitted light intensity I of the incident light intensity I_0 through the measuring media can be expressed by

$$\frac{I}{I_0} = \exp\left(-\int_0^L K\,ds\right) \tag{1}$$

where L is the optical path length, K the attenuation coefficient, $K = (\pi d_p^2/4)\,Q_e N$, d_p the particle diameter, Q_e the extinction efficiency factor and N the particle number density. The distribution of the value of K shown above must be determined for the calculations of gas and particle temperatures.

2.1.2. *Particle temperature distribution.* Radiation from burning pulverized coal particles were certified to follow the gray body radiation within the measuring wavelength by a spectroscopic analysis. Wien's approximation was applied to this radiating media at the wavelength of λ_1 (650 nm) and λ_2 (900 nm), the local temperature can be calculated from the local light intensities of $E(\lambda_1, T)$ and $E(\lambda_2, T)$ as expressed by

$$T_p = C_2\left(\frac{1}{\lambda_2} - \frac{1}{\lambda_1}\right) \Big/ \ln\left(\frac{E(\lambda_1, T_p)}{E(\lambda_2, T_p)}\right) \tag{2}$$

and

$$E(\lambda, T) = C_1 \lambda^{-5} \exp\left(-\frac{C_2}{\lambda T}\right) \tag{3}$$

where $E(\lambda,T)$ is the black body radiation of Wien's formula and C_1 and C_2 are the first and second constants which appear in Planck's black body radiation.

The light radiated from particles is attenuated and/or amplified by other particles along the optical path, and this effect must be taken into account to reconstruct the local particle radiations of $E(\lambda,T)$ for two wavelengths which lead the particle temperature distributions by equation (2).

2.1.3. *Gas temperature distribution.* A wing zone Na-D line reversal method was adopted to minimize the errors introduced by the self-absorption which occurred at the cooler boundaries. The intensity of the Na-D line from the gas was much stronger than that from the particles in the pulverized coal combustion field tested. This was checked by the spectroscopic analysis. We adopted a wavelength of $\lambda = 591.4$ nm at the wing region of the Na-D line spectrum and the gas temperature can be obtained by

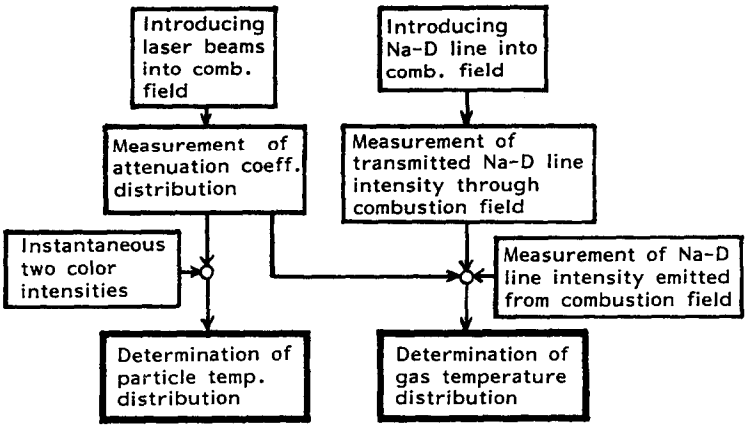

FIG. 1. Flow chart of measuring procedure.

$$\frac{1}{T_g}=\frac{1}{T_L}-\frac{\lambda}{C_2}\ln\frac{M_2}{I_0-M_1+M_2} \tag{4}$$

where T_L is the brightness temperature of the light source at λ

$$M_1=B\left(1-\exp\left(-\int K\,ds\right)\right)+I_0\exp\left(-\int K\,ds\right),$$

$$M_2=B\left(1-\exp\left(-\int K\,ds\right)\right)$$

B the local radiation intensity at gas temperature T_g and I_0 the radiation intensity of the light source at temperature T_L at λ. These equations show that the considerations of attenuation by particles along the optical path must again be considered for the determination of gas temperature distributions.

2.2. *Experimental system*

2.2.1. *Combustion furnace and tested coal.* A water cooled pulverized coal combustion furnace of 30 cm i.d. and 2.3 m length with downward flow with swirling air was fabricated for this experiment as shown in Fig. 2. Four pairs of optical measuring windows which could view the whole diameter of the combustion furnace were mounted along the flow direction. Ash was collected by a combination of an ash reservoir beneath the combustion furnace and a bagfilter system. The pulverized coal, the fineness of which was 100%–200 mesh through, was fed by an auto-coal-feeder at the rate of 3.6 kg h^{-1} and transported by a primary air flow into a burner set at the top of the furnace. A secondary air flow was introduced tangentially so as to surround the cone shaped injected coal cloud and give the swirling flow to promote the

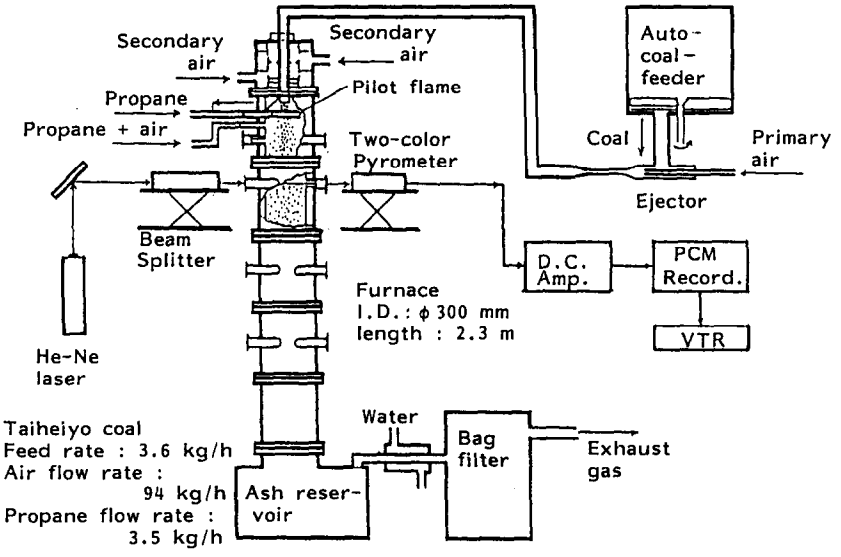

FIG. 2. Swirl flow pulverized coal combustion furnace.

Table 1. Properties of coal used

	Coal A	Coal B
Proximate analysis (%, dry):		
Volatile matter	44.4	29.5
Fixed carbon	39.8	62.2
Ash	15.8	8.3
Ultimate analysis (%, dry):		
C	65.4	77.3
H	5.47	3.98
O	12.5	9.0
N	0.79	0.79
S	0.21	0.70

mixing and stabilize the flame. Propane was fed to a circular shaped pilot burner which was located coaxially to the main burner.

The properties of the coals used in this experiment and the theoretical work are shown in Table 1, in which coal A is the domestic Taiheiyo coal and coal B the Chinese Datong coal. The former is known as a coal with a higher content of volatile matter, while the latter is one with a higher content of fixed carbon.

2.2.2. *Optical system.* The optical system adopted in this study is shown in Fig. 3. The system consists of an attenuation measurement by an incident He–Ne laser light, an instantaneous two color pyrometry and a wing zone Na-D line reversal device. In this experiment axi-symmetric distributions were confirmed by the time mean characteristics, and it was not necessary to rotate the optical system as in the case of medical CT scanning devices. The incident He–Ne laser beam was chopped by a sector and separated the information from the radiation from the particles. Four beams of divided He–Ne laser lights were introduced in a measuring plane. Four beams 5 mm in diameter of the Na-D line reversal method and the same number of beams (same diameter as above) of two color pyrometry were introduced simultaneously. These four beams were located so that they could cover the places for eight beam measurement if the axi-symmetric distributions were realized. Photodiodes converted the optical information into electric signals. The signals were recorded by a PCM recorder after amplification by a d.c. amplifier.

2.3. *Results and discussions*

Figure 4 shows the comparisons of time mean particles and gas temperature distributions (a) at an

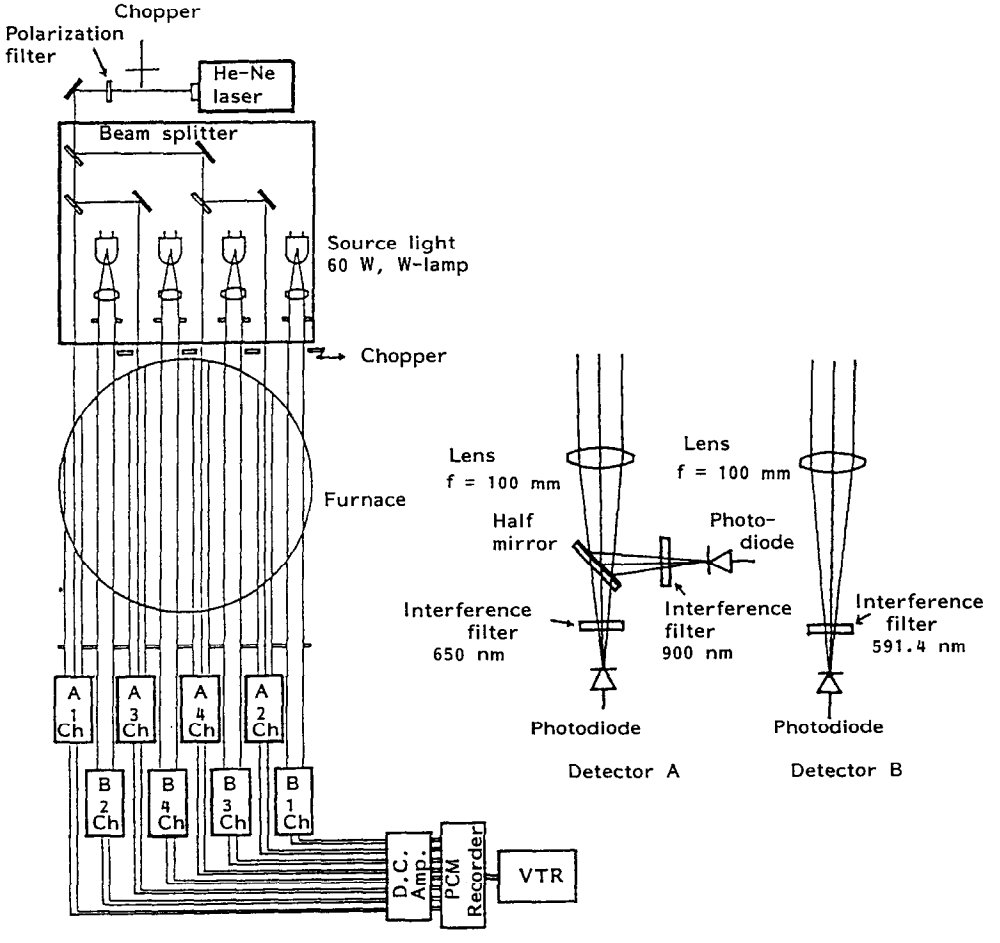

FIG. 3. Optical system.

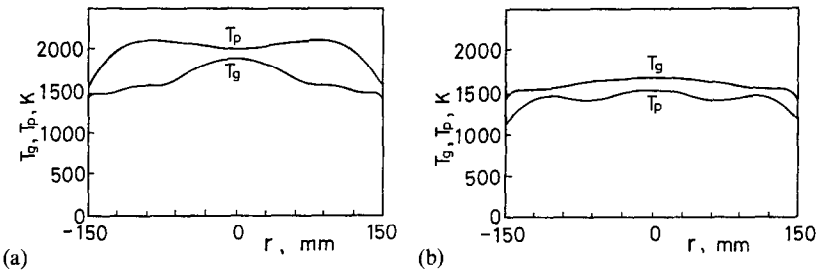

FIG. 4. Time mean particle and gas temperature distributions for coal A: (a) upper measuring port; (b) lower measuring port.

upper measuring port (675 mm downstream under a coal injector) and (b) at a lower port (1125 mm downstream under the coal injector). At the upper measuring port, the particle temperature shows the concave distribution near the center while the gas temperature has a convex distribution. This tells us that the time mean combustion region of coal particles is located out of the center line because of the selective consumption of oxygen in the primary air near the center line caused by the combustion of evolved volatile matter. At the main combustion region out of the center line, the combustion of both volatile matter and fixed carbon takes place on the surface or inside the coal particle [13]. Under these conditions the particle temperature could be higher than the gas temperature because of the high heat release rate compared to the heat loss from the particle. The maximum temperature difference between particle and gas is more than 500 K.

On the contrary, according to the mixing with the secondary air and the progress of volatile matter combustion, the combustion region propagates into the central area till the coal particles flow down to the lower port, and both the particle and gas temperature are convex in shape. The volatile matter might be almost consumed before reaching this region and the residual small amount of volatile matter and abundant fixed carbon burn here. The heat releasing rate is not as high as that at the upper port and the heat loss from the particles by radiation makes the particle temperature lower than the gas temperature. This tendency appears more clearly for the larger particles and the measured particle temperature could be considered as being weighed to that of larger particles.

3. PREDICTION OF PARTICLE AND GAS TEMPERATURES BY QUASI-ONE-DIMENSIONAL MODEL

In this section, temperature histories of burning particles and gas in a one-dimensional pulverized coal combustion process are separately predicted by a simplified mathematical model combining the two important processes of time-dependent change of flame structure around particles and radiative heat transfer in a media with homogeneously dispersed burning particles. First, radiative properties of scattering and absorbing are rigorously calculated by use of the Mie theory [11] for various types of particles appearing in the actual combustion process. Second, the dynamic behavior of the flame zone around the burning coal particles is analyzed. Then, combining those results with heat transfer analyses, temperature histories of particles and gas are calculated.

3.1. *Scattering and absorbing characteristics of particles*

Efficiency factors of absorbing and scattering, Q_a and Q_s, and phase function, Φ, were rigorously calculated by use of the Mie scattering theory [11] for the spherical raw coal, char and fly ash particles. The extinction efficiency factor, Q_e, is given as a sum of Q_a and Q_s. The complex refractive indexes defined as $m = n - i\kappa$ were assumed to be 1.9–0.1i, 1.93–1.02i, and 1.5–0.001i for raw coal, char, and fly ash particles, respectively, considering the values in the literature and electrical conductivity of each particle. Here, n and κ are the usual refractive index and absorption index, respectively, and κ is smaller for particles of lower electrical conductivity.

The representative results are shown in Figs. 5(a) and (b) for char and fly ash particles. The results for raw coal particles are almost the same as those for char particles. The wavelength is selected as 2 μm here as a representative one which gives the maximum black body radiation energy in the combustion zone of about 1500°C. As for the char particles as shown in Fig. 5(a), the forward scattering is selectively dominant and this tendency is stronger for the larger particle size parameters, X, defined as $X = \pi d_p/\lambda$, where d_p and λ are the particle diameter and wavelength, respectively. The albedo of scatter, ω_s, defined as $\omega_s = Q_s/(Q_a + Q_s)$, is about 0.6 for coal and char particles in this case. On the other hand, the scattering and absorbing characteristics of fly ash particles, shown in Fig. 5(b), are different from those of char particles and show a strong oscillation in the phase function and that the phase function tends to that of Rayleigh scattering. The albedo of scatter, ω_s, is larger than 0.9, which shows the large contribution of scattering in the radiative transfer process, in this case of fly ash particles.

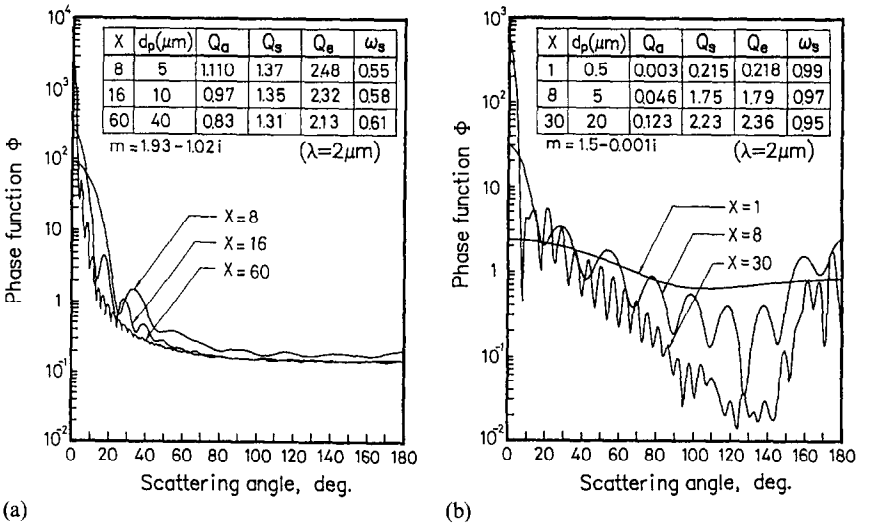

FIG. 5. Scattering and absorbing characteristics of particles: (a) char particle; (b) fly ash particle.

3.2. *Dynamic behavior of flame structure around particles*

The temperature histories of burning particles are affected not only by the radiative heat transfer process but also strongly by the time-dependent flame structural change around particles. When the evolving flux of volatile matter from the particle surface in the stage of volatile matter combustion is larger than the equivalent oxygen flux to the particle from surrounding air, the flame zone is pushed away from the particle surface. The feedback rate of the heat released in this flame zone to the particle is largely dependent on how distant the flame zone is from the particle surface. In this section, the dynamic behavior of the flame structure around particles is analyzed by a simplified model for the case where a single particle is immersed in the given high temperature air surrounded by the black body wall. The major assumptions applied in this analysis are (1) unsteady spherically symmetric phenomena, (2) a volatile matter evolution process of the first and single step Arrhenius type, (3) CH_4 as evolved volatile matter, (4) carbon oxidation by O_2 and CO_2 on the particle surface as the char reaction, (5) single step oxidation of CH_4 and CO as the gas phase reaction, and (6) transparent gas phase for radiative transfer. On the basis of the assumptions mentioned above, the time-dependent governing equations of the mass, energy and chemical species conservations for the gas phase, the solid phase mass conservations for the residual volatile matter, fixed carbon and ash in the particle, and the energy conservation for the particles have been simultaneously solved with the given initial and boundary conditions, as shown in detail in the literature [12].

Chemical and thermal structural changes around a particle were calculated with the time elapsed, t, after the exposure of a coal particle into hot air. The initial temperatures of the particle and hot air were set at 300 and 1500 K, respectively, and the wall temperature was fixed at 1800 K. The position of the flame zone was defined as that of the intersection of fuel and oxygen concentration profiles. It has been shown by this analysis that the flame zone moves with time away from the particle surface into the gas phase and then comes back to the surface with the decrease of volatile matter retained in the particle. The char combustion, in close proximity to, or on the particle surface, follows these processes.

The expansion behavior of the flame zone with time is shown in Fig. 6 for various initial particle diameters of 20, 40 and 100 μm. This result shows that the larger particle needs more time to be ignited and has the flame zone pushed farther away from the particle surface in the stage of volatile matter combustion, which is due to the larger flux of evolving volatile matter on the particle surface. These factors have a marked

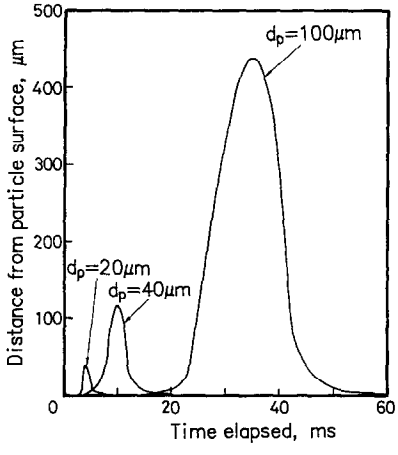

FIG. 6. Expansion of flame zone away from particle surface.

Table 2. Parameters of one-dimensional combustion furnaces

Furnace	A	B
length (m)	2.03	1.50
i.d. (mm)	140	80
wall structure	fire brick	water cooled with insulator coated
residence time (s)	0.5–1.0	0.2–0.7
heat load ($W\ m^{-3}$)	1.0×10^6	2.0×10^6
maximum temp (°C)	1500	1200

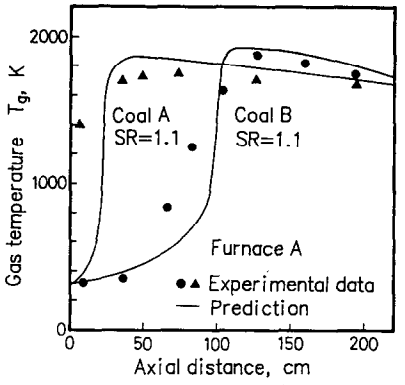

FIG. 7. Comparison of predicted and measured gas temperature profiles in furnace A for high volatile coal A and low volatile coal B.

effect on the temperature history of particles. A higher particle temperature is attained for the smaller particle, in this case, due to the fact that more heat released in the flame zone around the particle can be used to raise the particle temperature.

3.3. *Prediction of temperature histories of particles and gas in one-dimensional combustion furnaces*

Considering the two important results obtained in Sections 3.1 and 3.2, the temperature histories of particles and gas are numerically predicted for the one-dimensional pulverized coal combustion process in the two different types of furnaces, A and B, as shown in Table 2, which have been actually used for the experimental study [13] in our laboratory. The radiative heat transfer process was analyzed using the Monte Carlo method and detailed formulations including other processes of convection and conduction are described in the literature [12]. The particle size distributions of pulverized coal were assumed to be 30, 40, 30 wt.% of 10, 50, 100 μm particles for furnace A, and 30, 50, 20 wt.% of 20, 40, 100 μm particles for furnace B, respectively, considering those actually used in the experiments [13]. The air–fuel stoichiometric ratios, SR, were 1.1 and 1.2 for furnaces A and B, respectively. The complex refractive index and wavelength of thermal radiation were assumed to be $m = 1.93 - 1.02i$ and $\lambda = 2\ \mu$m, respectively, as the representative ones in the actual combustion furnace.

Figure 7 shows the comparison of the predicted gas temperature histories with the measured ones for the one-dimensional furnace A. The effect of the volatile matter content in the raw coal on the gas temperature profile is clearly shown in this figure for high volatile coal A and low volatile coal B. The fairly close agreement between the predicted and measured results as shown in Fig. 7 assures the validity of the model formulated in this study. Figure 8 predicts the particle temperature histories in furnace A for coals A and B. For high volatile coal A, the particle temperature of smaller particles is raised above that of larger particles in the early stage of volatile matter combustion, and then after the consumption of volatile matter, more rapidly decreases in the char combustion region, where the smaller particles have a lower temperature. The results for the smaller particles can be explained by the effects of the larger heat feedback to the particle from the surrounding flame zone in the volatile matter combustion region as mentioned in Section 3.2 and the relatively larger heat losses by convection and radiation from the particle to the gas and the wall in the char combustion region. The maximum particle temperature elevation attained above the mean gas temperature is 400 K for a particle diameter of 10 μm. On the other hand, for low volatile coal B, the particle temperature profile does not have such a steep peak as that of coal A, even in the volatile matter combustion region. The large temperature difference in the region of volatile matter combustion shown in Fig. 8 agrees well with the experimentally observed results in Fig. 4 including the temperature levels for coal A.

A close agreement between the analytical and measured mean gas temperatures is again shown in Fig. 9 for furnace B. Figure 10 shows the effect of initial particle size distribution on the gas temperature profile, where the solid line is the same as that in Fig. 9. The chain line and broken line show the results

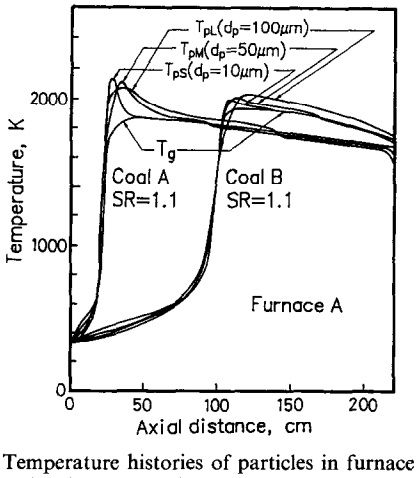

FIG. 8. Temperature histories of particles in furnace A for coals A and B. (T_{pL}, T_{pM} and T_{pS} are the particle temperatures for large, medium and small particles, respectively.)

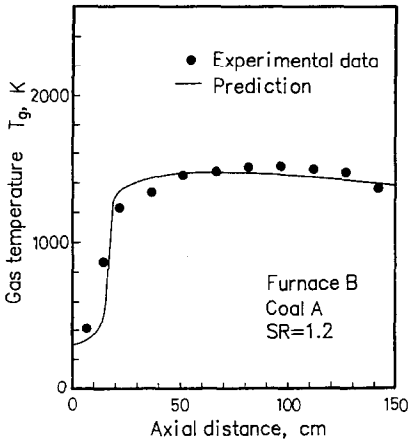

FIG. 9. Gas temperature profile in furnace B for coal A.

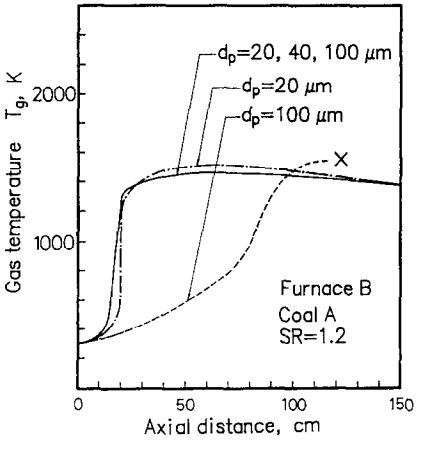

FIG. 10. Effect of particle size distribution of raw pulverized coal on the gas temperature profile.

obtained by assuming the mono-dispersed 20 and 100 μm particles, respectively. Though the mono-dispersed 20 μm particles have almost the same temperature profile as the solid line, for the mono-dispersed 100 μm particles, the solution converges to a normal room temperature, which shows that self-sustained combustion is impossible in the latter case. The results in Fig. 10 indicate an interesting aspect from the application standpoint. It could be possible to greatly improve the ignition and combustion characteristics of low combustible pulverized coal, by adding a small fraction of high combustible fine coal particles.

Figures 7–10 include the scattering effect in the radiative transfer process. The comparison between the results with and without scattering for the 100 μm particles under the same conditions of Fig. 9 was examined. Though significant differences up to 10% were seen in the preheating zone and the downstream region, the differences were quite small, as a whole, due to the selectively strong forward scattering process in the raw coal and char particles as shown in Fig. 5.

4. CONCLUSIONS

The following conclusions on the particle and gas temperature histories in the pulverized coal combustion process have been derived from the direct measurement of these temperatures by the optical CT technique and from theoretical calculations.

(1) The existence of temperature differences between particle and gas was clarified. The particle temperature is highly elevated above the surrounding mean gas temperature, especially in the region of volatile matter combustion.

(2) For high volatile coals, the particle temperature of smaller particles is higher in the volatile matter combustion stage, while lower in the char combustion stage compared to that of larger particles.

(3) Small particles less than about 20 μm originally contained in the pulverized coal largely enhance the radiative preheating and ignitability of the pulverized coal cloud.

(4) The effect of scattering on the particle temperature history is, as a whole, not so large (up to 10%), although the albedo of scatter of the particles is larger than 0.6. This is due to the selectively strong forward scattering like diffraction in the scattering process of raw coal and char particles.

Acknowledgement—The development of particle and gas temperature measurements by the optical CT technique has been carried out in cooperative research with Electric Power Development Co. Ltd., Mitsubishi Heavy Industries Co. Ltd. and Furukawa Electric Co. Ltd. The authors also gratefully acknowledge Mr H. Ichimaru, Mr K. Ueki and Mr K. Goto for their contributions to the development of the experimental apparatus and performance of the experiments. They would also like to thank Mr M. Takeshi for his contributions to the development of computer programs and for carrying out the calculations.

REFERENCES

1. M. Saitoh, M. Sadakata, M. Satoh, T. Saotome and T. Sakai, Particle temperature measurement in the pulverized coal combustion, *Proc. of 24th Japan Symp. on Combustion*, p. 178 (1986).
2. T. J. Love and R. J. Grosh, Radiative heat transfer in absorbing, emitting and scattering media, *Trans. ASME, J. Heat Transfer* **87C**(5), 161 (1965).
3. H. M. Hisia and T. J. Love, Radiative transfer between parallel plates separated by nonisothermal medium with anisotropic scattering, *Trans. ASME, J. Heat Transfer* **89C**(8), 197 (1967).
4. F. R. Steward and K. H. Guruz, The effect of solid particles on radiative transfer in cylindrical test furnaces, *Proc. 15th Symp. (Int.) on Combustion*, p. 1271 (1974).
5. T. F. Wall, A. Lowe, L. J. Wibberley, T. Mai-Viet and R. P. Guputa, Fly ash characteristics and radiative heat transfer in pulverized coal-fired furnaces, *Combust. Sci. Technol.* **26**, 107 (1981).
6. E. J. Kansa and H. Perlee, A transient dust-flame model: application to coal-dust flames, *Combustion Flame* **38**, 17 (1980).
7. S. P. Mussara, T. H. Fletcher, S. Niksa and H. A. Dwyer, Heat and mass transfer in the vicinity of a devolatilizing coal particle, *Combust. Sci. Technol.* **45**, 289 (1986).
8. M. Jost, I. Leslie and C. H. Kruger, Flow-tube reactor

studies of devolatilization of pulverized coal in an oxidizing environment, *Proc. 20th Symp. (Int.) on Combustion*, p. 1531 (1984).
9. S. F. Green, An acoustic technique for rapid temperature distribution measurement, *J. Acoust. Soc. Am.* 77(2), 759 (1985).
10. F. Itoh and M. Sakai, Fundamental studies of acoustic measurement and reconstructing combustion temperature in large boilers, *JSME* (Ser. B) **53**(489), 1610 (1987).
11. H. C. Van De Hulst, *Light Scattering by Small Particles*, Chap. 9. Dover, New York (1985).
12. M. Takeshi, Radiative heat transfer process and particle temperature in pulverized coal combustion, Master's Thesis, Toyohashi University of Technology (1987).
13. K. Okazaki, H. Shishido, T. Nishikawa and K. Ohtake, Separation of the basic factors affecting NO formation in pulverized coal combustion, *Proc. 20th Symp. (Int.) on Combustion*, p. 1381 (1984).

MESURE OPTIQUE CT ET PREVISION MATHEMATIQUE DE LA TEMPERATURE DANS UNE COMBUSTION DE CHARBON PULVERISE

Résumé—Les distributions de température de particules et de gaz dans la combustion de charbon pulvérisé sont mesurées par une nouvelle technique CT (tomographie par ordinateur) dans laquelle la température de particule est atteinte par une pyrométrie instantanée à deux couleurs et la température du gaz par une méthode inverse de ligne Na-D. Un modèle mathématique simple est formulé pour une combustion monodimensionnelle de charbon pulvérisé avec transfert radiatif et mécanismes de diffusion, d'absorption et d'émission. Les calculs conduisent à des températures de particules supérieures de 400 K à celles du gaz, spécialement dans la région de combustion des matières volatiles. Ceci explique bien les observations faites par les mesures optiques.

OPTISCHE COMPUTER-TOMOGRAFIE-MESSUNG UND BERECHNUNG DES TEMPERATURFELDES BEI DER VERBRENNUNG FEINGEMAHLENER KOHLE

Zusammenfassung—Die Temperaturverteilungen von Partikeln und Gas bei der Verbrennung von feingemahlener Kohle in einem Ofen wurden mit einem neuentwickelten Computer-Tomografie-Verfahren gemessen. Hierbei wurde die Partikeltemperatur mit einem Momentan-Zweifarben-Pyrometer und die Gastemperatur mit einer Flügelzonen-Na-D-Linienumkehrmethode gemessen. Ein vereinfachtes mathematisches Modell wurde für die eindimensionale Verbrennung feingemahlener Kohle formuliert. Es berücksichtigt die Streuung, die Absorption und die Emission beim Wärmeübergang durch Strahlung. Die Modellrechnungen ergaben eine um 400 K höhere Temperatur der Partikel gegenüber dem Gas, besonders im Bereich der Verbrennung der flüchtigen Materie. Dieses Ergebnis erklärte die bei den optischen Messungen beobachteten Phänomene.

ОПТИЧЕСКИЕ КОМПЬЮТЕРНО-ТОМОГРАФИЧЕСКИЕ ИЗМЕРЕНИЯ И МАТЕМАТИЧЕСКИЙ РАСЧЕТ ПОЛЕЙ ТЕМПЕРАТУР ПРИ ГОРЕНИИ УГОЛЬНОЙ ПЫЛИ

Аннотация—Распределения температур частиц и газа в топке, сжигающей угольную пыль, измерялись недавно разработанным КТ (компьютерно-томографическим) методом, в котором температура частицы измерялась с помощью мгновенной двухцветной пирометрии, а температура газа—методом обращения крыльев линии Na – D. Упрощенная математическая модель горения угольной пыли, учитывающая процессы радиационного теплообмена—рассеяние, поглощение и излучение—сформулирована для одномерной области горения. Расчеты с помощью модели показали, что температура частицы более чем на 400 К выше температуры газа в особенности в области горения летучего вещества. Данный результат хорошо объясняет явления, наблюдаемые при оптических измерениях.